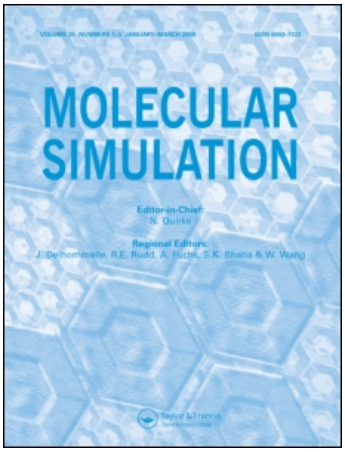

Molecular Simulation
Publication details, including instructions for authors and subscription information:
http://www.informaworld.com/smpp/title~content=t713644482

Atomistic simulations of isotactic and atactic poly(methyl methacrylate) melts: exploring the backbone conformational space

Karl N. Kirschner[a]; Kathrin Heikamp[a]; Dirk Reith[a]
[a] Department of Simulation Engineering, Fraunhofer-Institute for Algorithms and Scientific Computing SCAI, Sankt Augustin, Germany

First published on: 05 November 2010

To cite this Article Kirschner, Karl N. , Heikamp, Kathrin and Reith, Dirk(2010) 'Atomistic simulations of isotactic and atactic poly(methyl methacrylate) melts: exploring the backbone conformational space', Molecular Simulation, 36: 15, 1253 — 1264, First published on: 05 November 2010 (iFirst)
To link to this Article: DOI: 10.1080/08927020903536374
URL: http://dx.doi.org/10.1080/08927020903536374

Molecular Simulation
Vol. 36, No. 15, December 2010, 1253–1264

Taylor & Francis
Taylor & Francis Group

Atomistic simulations of isotactic and atactic poly(methyl methacrylate) melts: exploring the backbone conformational space

Karl N. Kirschner*, Kathrin Heikamp and Dirk Reith

Department of Simulation Engineering, Fraunhofer-Institute for Algorithms and Scientific Computing SCAI, Schloss Birlinghoven, 53754 Sankt Augustin, Germany

(*Received 1 September 2009; final version received 7 December 2009*)

Molecular dynamics simulations were performed separately on an isotactic poly(methyl methacrylate) (PMMA) melt and on an atactic PMMA melt. These simulations allow for a detailed atomistic exploration of the conformational space about the polymers' backbone at a temperature above the glass transition for both polymers, which is experimentally difficult to accomplish. In agreement with previous experimental and theoretical studies, we found the *trans–trans* backbone conformation to be the most energetically stable, followed by the *trans–gauche* conformations. Unique in this study is the ability to attribute how the underlying meso and racemic diad pairs contribute to the overall backbone population. Additional simulations were performed on methyl methacrylate, the compound that forms PMMA through radical reactions. These latter simulations help to validate our recently created force field for use in condensed-phase simulations.

Keywords: poly(methyl methacrylate); methyl methacrylate; molecular dynamics

1. Introduction

Poly(methyl methacrylate), also known as Plexiglas or PMMA, is a common commercial polymer that has a vast range of uses and applications. It is formed through a radical polymerisation process involving methyl methacrylate (MMA). By varying the experimental conditions, PMMA can be easily formed with three different tacticities: isotactic (i-PMMA), syndiotactic (s-PMMA) and atactic (a-PMMA) configurations. Tacticity arises from enantiomeric atoms in a polymer's backbone. An isotactic configuration consists of residues with the same enantiomeric configuration, while a syndiotactic configuration has residues with alternating enantiomeric configurations. Both isotactic and syndiotactic polymers are called stereoregular polymers due to their repeating residue configuration. Atactic polymers are stereoirregular because they have a random distribution of enantiomeric centres throughout the polymer chain. PMMA is an excellent example of how tacticity affects the polymer's chemical observables. Two chemical properties that exemplify this are the glass melting temperature (T_g of $\sim$50 and $\sim$105°C for i- and s-PMMA) [1] and chain stiffness (characteristic ratio C_∞ of 10.2 and 7.2 Å^2 for i- and s-PMMA) [2].

Structural and energetic investigations on PMMA have a long experimental [3–17] and theoretical [2,11–13,18–24] history. Unlike small molecules (e.g. butane, propanal, etc.), it is very difficult to obtain detailed structural and energetic information on a single polymer molecule. Experimentally, the most useful techniques have been X-ray diffraction, neutron diffraction and variable temperature infrared spectroscopy. Theoretically, force field-based methods are the most common since the system size that is required to properly capture the polymer's local chemical environment, both inter- and intramolecular, has largely prohibited quantum mechanical studies. By surveying the current literature, it is clear that understanding the structure and dynamics of PMMA and other polymers at atomic resolution remains a challenging research area [25].

Partly due to the experimental difficulties of investigating a polymer's structure at atomic resolution, the polymer's chemical and physical characteristics are often attributed to its morphology or basic chemical structure, not to its three-dimensional atomic structure. At an atomistic level, some of the chemical properties are influenced by the conformations that the individual molecules adopt. Subsequently, the conformation is partly governed by the polymer's tacticity. For example, one can imagine that an isotactic polymer adopts a different set of conformational families along its backbone atoms in comparison to an atactic polymer. Experimentally, it has proven difficult to obtain definitive information on the PMMA's backbone conformation, especially so when it exists in an amorphous state [16]. The predominant conclusion made by several experimental groups, and supported by theory, is that i- and s-PMMA occur mainly in a *trans–trans* backbone conformation, as measured in the solid state or dissolved in organic solvents [2,12,14–17,24,26]. However, this does not negate the presence of the *gauche* conformations, which are believed to occur at a

*Corresponding author. Email: karl.kirschner@scai.fraunhofer.de

ISSN 0892-7022 print/ISSN 1029-0435 online

DOI: 10.1080/08927020903536374
http://www.informaworld.com

low percentage below T_g and increases at temperatures above T_g [19,26,27].

We present here a molecular dynamics (MD) study on two systems, an isotactic PMMA melt and an atactic PMMA melt. Our goal is to explore the allowed and disallowed conformational space of the backbone torsion angles at a temperature well above the glass transition temperature for both systems. A new force field will be employed that has recently been developed in our group, whose performance will be partially validated by performing the MD simulation on MMA, the chemical building block of PMMA, and whose results will be compared to experimental observables.

2. Methodology

The force field used in this study is an extension of the Glycam06 force field for carbohydrates [28]. The general philosophy of the new force field, and of Glycam06, is that: (a) it be transferable between chemical systems, (b) the partial atomic charges on aliphatic hydrogens are summed into their adjoined carbon atom and (c) explicit parameter terms are used to account for all bond, angle and torsion connectivities (i.e. no generic torsion terms).

The conformational space of MMA was explored by rotating around each heavy atom torsion, followed by minimisation and a frequency analysis performed at the HF/6-31G(d) level of theory to ensure that the optimised geometry was a minimum on the potential energy surface. The partial atomic charges were determined using the restrained electrostatic potential (RESP) methodology [29] by fitting to an electrostatic potential, created for each minimum using the HF/6-31G(d) level of theory and the CHELPG formalism, with a restraint weight of 0.01 [28]. The resulting charges were Boltzmann weighted, at a temperature of 298.15 K, using the relative energy of the minima as computed by the HF/6-31G(d) level of theory [15].

Four residue types were created for PMMA. Two residue types were used to cap the polymer's beginning and end, while two more were required to represent the enantiomeric centres for the internal residues. 2-Methylpropyl acetate was used to develop the charges for all four PMMA residue types, using the same quantum mechanical and RESP procedure described for MMA.

A non-bonded cut-off of 10.0 Å, or $\sim 5\sigma(C_{sp^3})$, was used for all MD calculations, while electrostatic interactions at longer distances were computed using the particle mesh Ewald method [30, 31]. Non-bonded and electrostatic scaling factors were set to 1.0, which is consistent with the development of the Glycam06 force field. Temperature regulation was controlled using Langevin dynamics with a collision frequency of 1.0 ps^{-1} and a unique random-prime-number seed was used at each restart point. The SHAKE algorithm was used to constrain all bonds that include hydrogen atoms, and subsequently these bonds were excluded from the force evaluations [17]. A time step of 0.002 ps was used throughout all simulations. For the periodic boundary condition (PBC) simulations, the pressure was kept constant at 1 bar with a relaxation time of 1.0 ps.

Two model systems were constructed for MMA: a single MMA molecule for gas-phase simulations and 525 molecules for PBC simulations. The PBC simulation was heated from 5 to 298 K in 50 ps, followed by 5 ns at 298 K. Additional short simulations ($\sim$2 ns) were performed at temperatures of 280, 360, 400 and 450 K. Enthalpies of vaporisation (ΔH_{vap}) were determined at each of these temperatures using the following formula [32]:

$$\Delta H_{vap} \approx \langle \Delta PE_{\text{single-molecule gas-phase MD}} \rangle - \frac{1}{n} \langle \Delta PE_{\text{PBC MD}} \rangle + RT, \quad (1)$$

where n is the number of molecules, R is the ideal gas constant, T is the temperature and ΔPE is the potential energy of the system.

The heat capacity for MMA was determined by computing the system's enthalpy (H) at various temperatures, and determining the slope of the resulting straight-line fit in a plot of ΔH vs. temperature, as governed by the following equation:

$$C_P \approx \frac{1}{n} \left(\frac{\partial(\langle H \rangle)}{\partial T} \right)_P = \frac{1}{n} \left(\frac{\partial(\langle \Delta PE \rangle + P\langle V \rangle)}{\partial T} \right)_P, \quad (2)$$

where P is the pressure and V is the volume.

For PMMA, two model systems were constructed, one isotactic and atactic, each containing 59 polymers whose lengths were eight residues long. The atactic model was generated such that each residue, within each of the 59 polymers, was randomly assigned an enantiomeric configuration. Thus, each polymer chain contains different randomised diad sequences. The starting configuration had the polymers arranged in a crystal lattice-like pattern. The non-capping residues possess enantiomeric centres as shown in Figure 1, which have been somewhat arbitrarily designated as D and L following the convention of Flory and co-workers [2,14,33]. Minimisations were performed using 50 cycles of the steepest descent method, followed by the conjugate gradient method until a convergence of less than 1 kcal mol^{-1} $Å^{-1}$ was obtained. Each MD simulation on PMMA was performed using PBCs. For the first system studied, i-PMMA, a series of annealing and equilibration steps were performed for a total of 167 ns (Figure 2). Using the knowledge gained from this simulation, the a-PMMA was heated from 5 to 900 K in 50 ps, followed by an $\sim$2 ns simulation at this high temperature, and then cooled to 450 K in another 50 ps. The simulation was subsequently run for 65 ns at 450 K. Energetics, volume, pressure, density

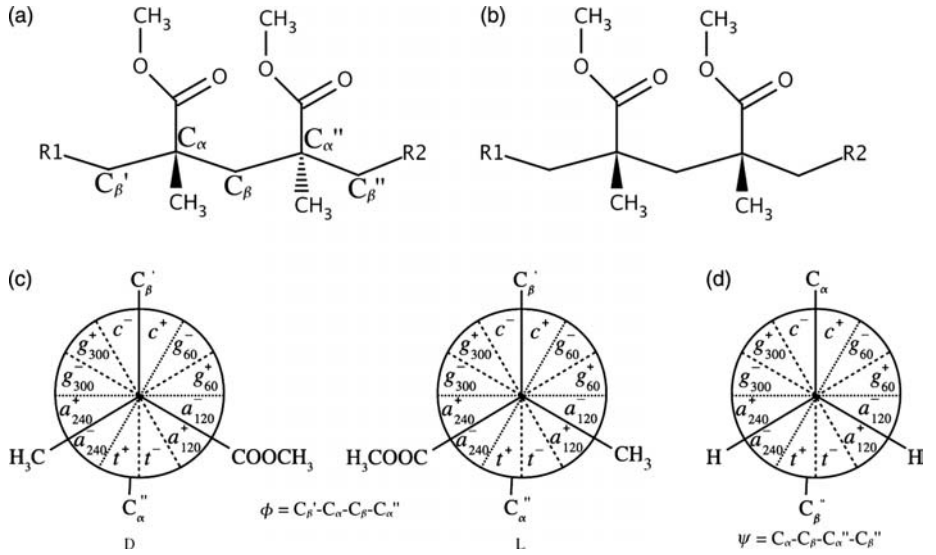

Figure 1. Representation of (a) an atactic and (b) an isotactic dyad in the PMMA polymer molecules. Conformations for the 'D' and 'L' enantiomeric configurations along the backbone torsion angles (c) ϕ and (d) ψ.

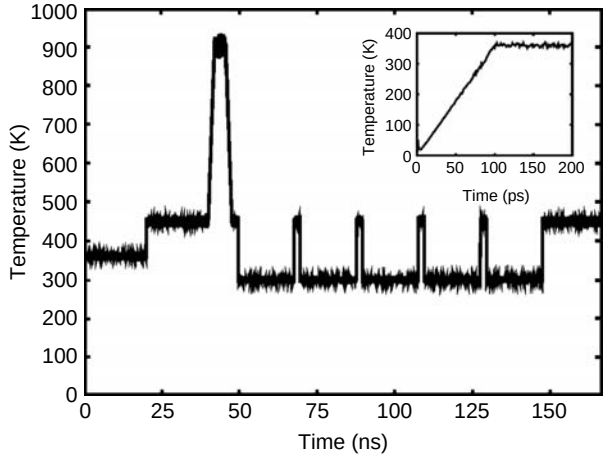

Figure 2. Temperature profile for the 167 ns simulation of 59 i-PMMA, with each polymer composed of eight residues. Insert shows a detailed view from 1 to 200 ps.

and temperature were monitored throughout the simulation as an indication of simulation and model stability.

All RESP charge derivations, molecular mechanics minimisations and MD simulations were performed using the AMBER9 software package [34]. All quantum mechanics calculations were performed using the GAMESS software [35]. Analysis of the MD simulations was performed using the ptraj code [34]. Production data for both i- and a-PMMA melts were taken from the last 20 ns in each simulation. The PMMA population histograms for the backbone ϕ and ψ torsion angles, as defined in Figure 1, were created using 5° bins, while the free energy surface (i.e. the potential of the mean force) [36] about these torsion angles was computed using

$$\Delta G = -RT \ln(\text{population}). \quad (3)$$

3. Results and discussion

3.1 Charge derivations

Two MMA conformations (Figure 3(a), (b)) were found to have significant Boltzmann populations at 298.15 K, both corresponding to a minimum in the ester side-chain rotation, with the methoxy group (i.e. $H_3CO{-}R$) maintained in the *trans* conformation. This is in full agreement with several experimental studies on MMA [37–39]. The HF global minimum has the ester oxygen *cis* to the carbon–carbon double bond, while the alternative *trans* conformation was found to be 0.33 kcal mol^{-1} higher in energy. There is disagreement in the literature, in both experimental and theoretical studies, as to which conformational is the preferred conformation [37, 39–41]. In order to remain consistent with the force field development, we chose the HF results to determine the partial atomic charges. The resulting partial atomic charges (Figure 4(a)) reflect a 64:36% Boltzmann population distribution between these two conformations. Deriving reliable partial atomic charges using a Boltzmann distribution represents a first approximation in capturing the quantum effects that are inherent upon conformational changes (e.g. intramolecular polarisability by neighbouring functional groups).

Even though the MMA molecule is the chemical precursor to PMMA, it is structurally and chemically different from a PMMA residue. The internal residues in a PMMA polymer are more structurally and chemically similar to 2-methylpropyl acetate (Figure 3(c), (d); R1 = R2 = H in Figure 4(d), (e)), and is therefore a more

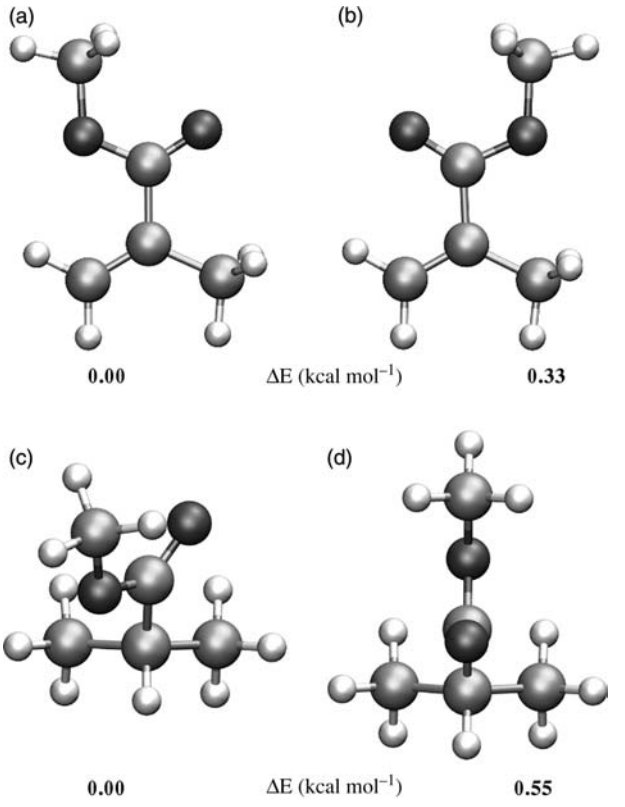

Figure 3. (a) and (b) MMA and (c) and (d) 2-methylpropyl acetate conformations used for Boltzmann weighting the partial atomic charge derivations. Relative energies were computed at the HF/6-31G(d) level of theory.

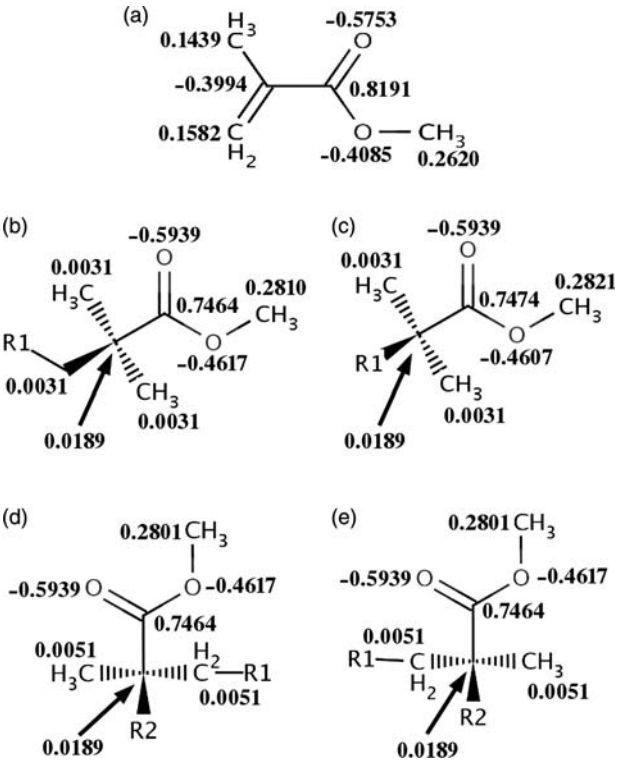

Figure 4. Partial atomic charges for (a) MMA, (b) beginning capping PMMA residue, (c) terminal capping PMMA residue, (d) 'enantiomer-D' PMMA residue and (e) 'enantiomer-L' PMMA residue.

appropriate candidate for the development of PMMA residues' partial atomic charges. There are two equivalent *gauche* conformations in 2-methylpropyl acetate, as defined by its O═C—C—H torsion angle; therefore, only one was counted in the Boltzmann statistics to avoid double counting of this conformation when transferred to a PMMA residue. A second unique conformation (with a *cis* O═C—C—H torsion angle) was found to be $0.55\,\text{kcal mol}^{-1}$ less stable, resulting in a *gauche*:*cis* population distribution of 72:28%. The resulting Boltzmann-weighted charges were then transferred to the capping and non-capping PMMA residues such that each residue's overall charge remained zero (Figure 4(b)–(e)).

3.2 MMA MD simulations

An autocorrelation coefficient was computed for the simulations performed at each temperature. The vector used to compute the autocorrelation represents the bond that would normally connect the ester side chain of PMMA to its backbone atoms once MMA had polymerised. At the lowest simulated temperature, 280 K, the molecule's translational and rotational motion became decoupled from its initial position after ~60 ps (Figure 5(a)). As expected, the time necessary for decoupling decreases as the temperature increases, reaching its smallest value of approximately 5 ps at 440 K (Figure 5(b)). From this analysis, it appears that the 2 ns simulations were long enough to provide a sufficiently randomised spatial orientation of the 525 MMA molecules to calculate density and enthalpy of vaporisation.

The experimental density has been determined by several groups, whose value ranges from 0.936 to $0.943\,\text{g cm}^{-3}$ at 298.15 K [42–45]. Our simulation provides a density of $0.942\,\text{g cm}^{-3}$ at this temperature, which agrees with the larger experimental values. As a function of temperature, the density displays the expected trend of decreasing values with increasing temperature, ranging from $0.962\,\text{g cm}^{-3}$at 280 K to $0.757\,\text{g cm}^{-3}$ at 440 K.

ΔH_{vap} is also experimentally known at several temperatures, ranging from 280 to 440 K [43]. Our computed ΔH_{vap} values for temperatures 280.0, 298.15, 360.0 and 440.0 K have an average error of +8.5% with respect to the experimental values (Figure 6). The experimental heat capacity (C_p) values range from 188.5 to $215.3\,\text{J mol}^{-1}\,\text{K}^{-1}$ [46–49]. We predict a value of

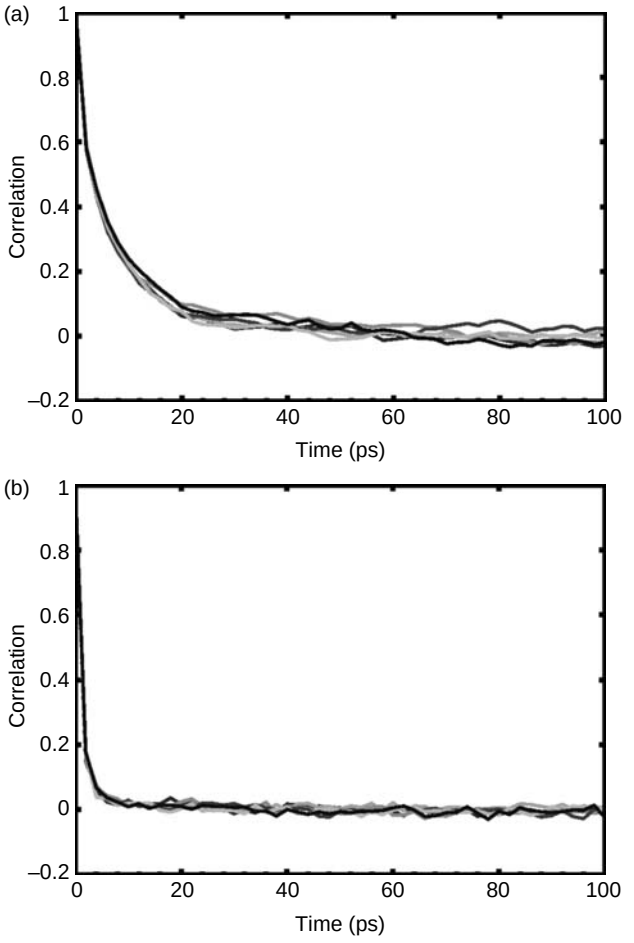

Figure 5. The autocorrelation coefficient of a vector formed between atoms C_2 and C_3 as a function of time for six MMA molecules. Graphs represent the simulations performed at (a) 280 and (b) 440 K.

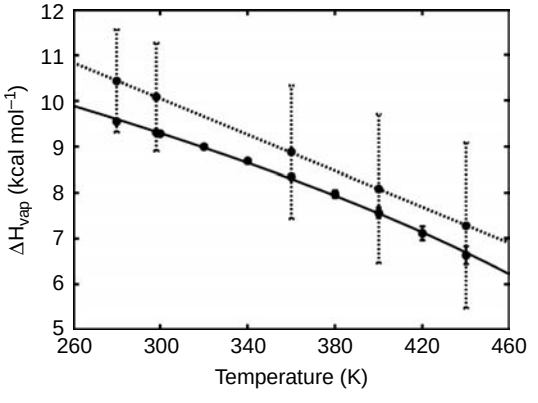

Figure 6. Experimental (solid line) and computed (dashed line) ΔH_{vap} for MMA at various temperatures.

213.9 J mol^{-1} K^{-1} using the data obtained from the 280.0, 298.15 and 360.0 K simulations, which are temperatures that reside in one phase for MMA.

Taking the above MMA results, it appears that our force field and the derived partial atomic charges adequately model the physics of MMA. However, it is apparent that we slightly overestimate the intermolecular binding energy since all three measured parameters (density, ΔH_{vap} and C_p) are higher than their average experimental values. This information will be used in future force field improvements, specifically in the refinement of Lennard-Jones parameters and the partial atomic charges. Nevertheless, these results, as well as those obtained in our force field validation suite (data forthcoming in a separate article), give us confidence that our current parameters and model development procedure are adequate to explore the conformational space of iso- and atactic PMMA using MD simulations.

3.3 PMMA MD simulations

3.3.1 Equilibration issues

Simulations of a polymer melt require additional equilibration steps vs. those normally done for small molecules due to the longer time scales required for translation, rotation and end-to-end chain reorientation motion. The initially built PMMA models have the individual polymers oriented in an artificial crystal lattice. Entropy was introduced into the model through a series of annealing steps for i-PMMA (Figure 2). Analysis of these annealing steps revealed that the simulation performed at 900 K provided the most widespread conformational sampling of each polymer in the melt. The annealing steps performed at 450 K relaxed the more local, or short-range, intra- and intermolecular residue contacts. As expected, the simulation at 298 K revealed less torsional motion in the polymers, and provided very minimal changes to the model's entropy. With this knowledge, we revised our simulation protocols for a-PMMA to include a ~2 ns simulation at 900 K, followed by a 65 ns simulation at 450 K. While the simulations presented here do not properly capture an individual polymer diffusion or rotation motion, which could be captured through coarse-grained simulations, the backbone torsion angles should be fairly well sampled by the annealing procedures described above.

We have verified that the torsion angles are adequately sampled by plotting several backbone torsion angles as a function of the entire simulation time (data not shown). From these plots, it is clear that these angles undergo several transitions during the annealing and production phases. Furthermore, we also monitored the polymers' end-to-end distances, which show large fluctuations between ~6 and ~17 Å during the production runs, indicating substantial motion in the polymers' backbone torsion angles. Finally, we have validated the simulations' time lengths that are adequately converged by examining the autocorrelation of the vector formed between the terminal residues of each polymer chain, and the

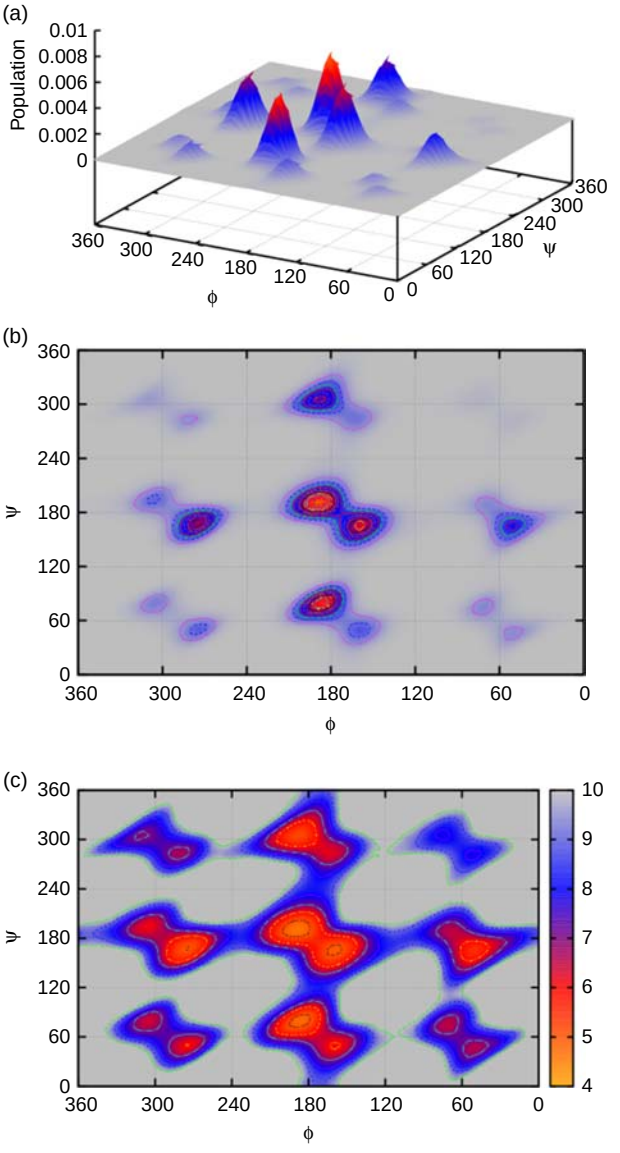

Figure 7. (a) Three-dimensional and (b) two-dimensional projection of the population distribution for i-PMMA's backbone ϕ and ψ torsion angles at 450 K. (c) The two-dimensional projection of the total free energy (kcal mol^{-1}) surface about the ϕ and ψ torsion angles, as derived from the populations.

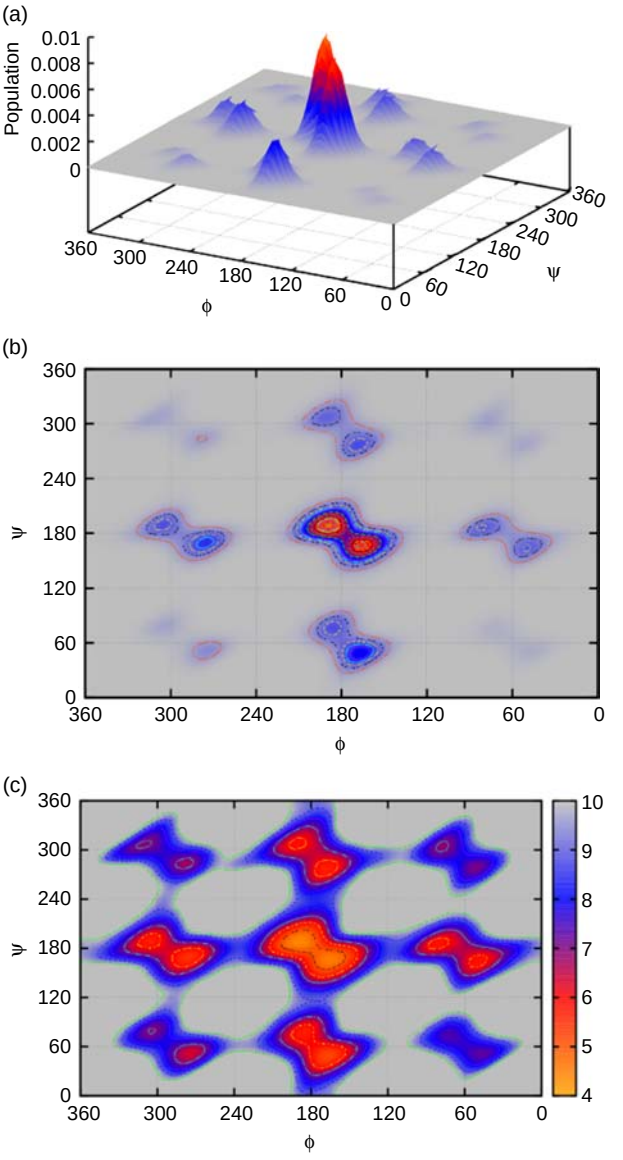

Figure 8. (a) Three-dimensional and (b) two-dimensional projection of the total population distribution for a-PMMA's backbone ϕ and ψ torsion angles at 450 K. (c) The two-dimensional projection of the total free energy (kcal mol^{-1}) surface about the ϕ and ψ torsion angles, as derived from the populations. The individual diad contributions to these figures are shown in Figure 9.

autocorrelation of the vector that represents the side-chain orientation. On average, an autocorrelation coefficient of 0.5, for both vector types, is reached within ~20 ns of the simulation, and continues to converge towards zero as the simulation progresses, indicating that our simulations' time lengths are adequate for this study.

3.3.2 *Allowed regions*

Based on the i- and a-PMMA population diagrams (Figures 7–9), an interesting trend is seen in the ϕ and ψ populations. There are nine generally accessible regions in the ϕ/ψ space that corresponds to *trans*, (+)-*gauche* and (−)-*gauche* for each angle. These regions can be qualitatively described using the nomenclature presented in Figure 1(c) and (d). The *cis* and *anticlinal* torsional angles do not possess any minima and represent regions of the ϕ/ψ space that are (a) interconversion pathways between conformational species and (b) high-energy states that are unlikely to be sampled at 450 K (Figures 7(c) and 8(c)). The nine populated regions and the areas of

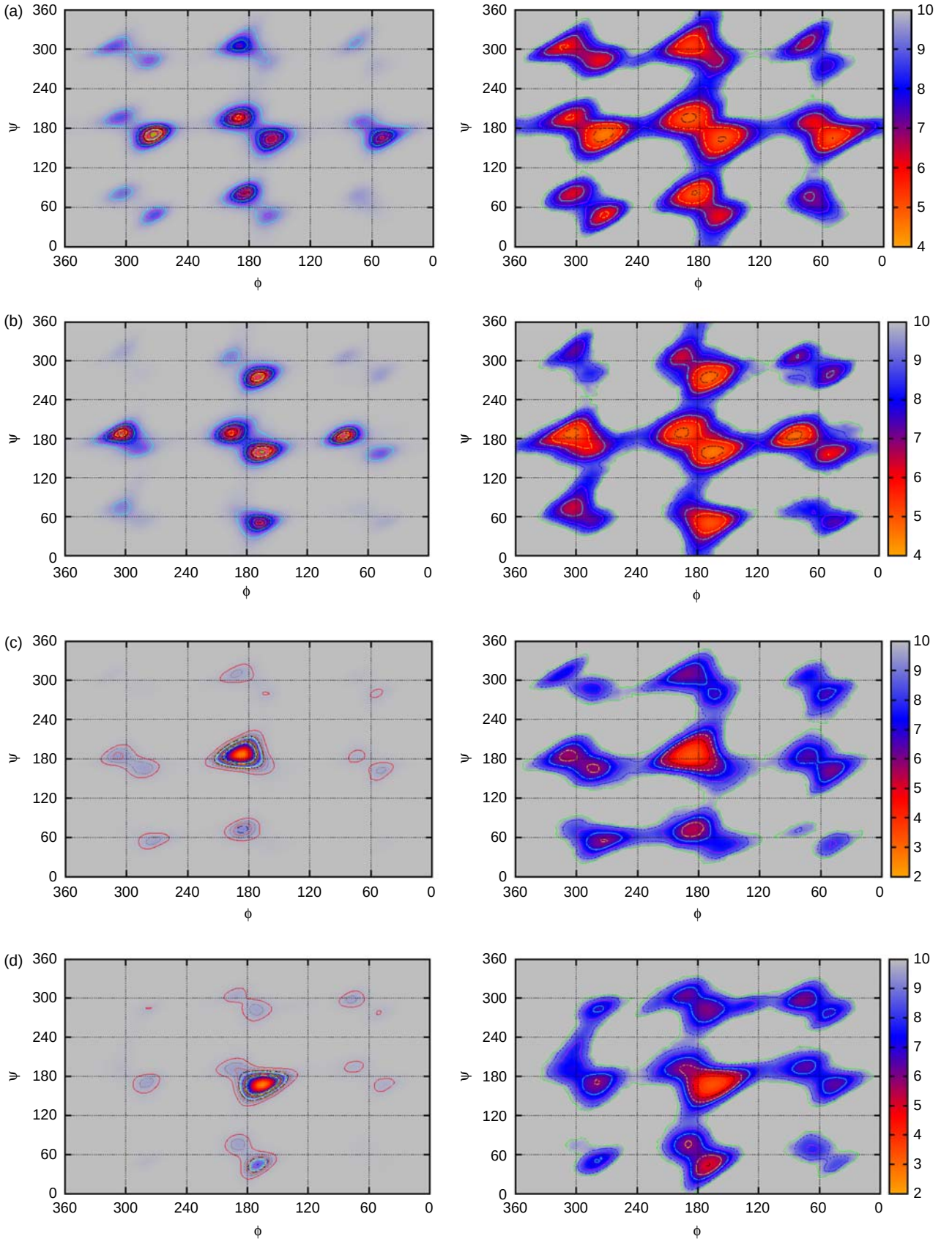

Figure 9. Two-dimensional projection of the population distribution and free energy (kcal mol^{-1}) surface for a-PMMA's diad pairs as a function of the backbone ϕ and ψ torsion angles. (a) D–D diad pair, (b) L–L diad pair, (c) D–L diad pair and (d) L–D diad pair.

higher energy occur due to the sp^3 hybridisation of the backbone atoms. The *trans* and *gauche* conformations represent atomic spacial arrangements that minimise steric hindrance, while the *cis* and *anticlinal* conformations have significant van der Waals repulsion due to eclipsing atoms.

The general consensus is that i-, a- and s-PMMA have a preferred *trans–trans* (i.e. $t|t$) backbone conformation at temperatures below their respective T_g [10,12, 26, 50]. It has also been experimentally shown that a population increase in the *gauche* conformation occurs at temperatures above T_g [26, 27]. Currently, experiments can only distinguish between the *trans* and *gauche* backbone conformations. The experimental difficulty in obtaining the finer details of the PMMA's conformation can be partially understood by considering the symmetry relationship between ϕ and ψ. Both angles contain only C_α and C_β atoms, but differ in their associated residues (Figure 1(a), (c) and (d)). Furthermore, the ψ angle is the reverse sequence of the ϕ angle, and they are identical if one does not consider which residues their constituent atoms belong to (i.e. ϕ: $C_{\beta'}$—C_α—C_β—$C_{\alpha''} \equiv \psi_{\text{reverse}}$: $C_{\beta''}$—$C_{\alpha''}$—$C_{\beta\text{-}\beta''}$—$C_{\alpha''}$—C_β—C_α). Experimentally resolving the ϕ and ψ angles would require detailed resolution of the individual atoms, which is very difficult to accomplish for an amorphous or melt sample. Fortunately, this is trivial to achieve in atomistic MD simulations and allows for the nine conformational regions to be resolved in a ϕ/ψ plot (Figures 7 and 8) using the nomenclature presented in Figure 1(c) and (d). For clarity, we use the $\{t|g + g|t\}$ notation to indicate a quantity that is the sum of all $t|g$ and $g|t$ regions (i.e. $\{t|g + g|\ t\} = (t|g_{60}) + (t|g_{300}) + (g_{60}|t) + (g_{300}|t)$), which can be compared directly to the *trans–gauche* conformations reported in the experimental literature.

The MD simulations predict the $t|t$ conformation to be lowest in energy for both i- and a-PMMA, resulting in populations of 34 and 45% at 450 K (Table 1). However, the *trans–gauche* conformations, $\{t|g + g|t\}$, have a total of four accessible local minima (i.e. $t|g_{60}$, $t|g_{300}$, $g_{60}|t$ and $g_{300}|t$), resulting in an overall $\{t|g + g|t\}$ population of 54 and 45% for i- and a-PMMA. The temperature dependence of the $t|t$ to $\{t|g + g|t\}$ ratio is given by the Boltzmann equation

$$\frac{N_{\{t/g+g/t\}}}{N_{t/t}} = 4\exp\left(\frac{-(E_{\{t/g+g/t\}} - E_{t/t})}{RT}\right). \qquad (4)$$

The factor of four represents the statistical weighting factor of the four accessible local *trans–gauche* conformations observed in the MD simulations. Thus, at even higher temperatures, the *gauche* contributions will increase since those minima become more accessible.

The simulated ΔG energy difference, for the nine regions of conformational space, ranges from 0.6 to 1.4 kcal mol^{-1}, depending on which the *trans–gauche* (i.e. $g_{60}|t$, $t|g_{60}$, $t|g_{300}$ and $g_{300}|t$) conformation is used in

Table 1. Populations and the corresponding relative free energies (kcal mol^{-1}) of i- and a-PMMA.

	i-PMMA		a-PMMA									
	Total		Total		D−D pair		L−L pair		D−L pair		L−D pair	
Conformation	Pop. %	Rel. ΔG°	Pop. %	Rel. ΔG°	Pop. %	Rel. ΔG°	Pop. %	Rel. ΔG°	Pop. %	Rel. ΔG°	Pop. %	Rel. ΔG°
$g_{60}\|g_{60}$	3.6	2.0	1.7	2.9	1.6	2.6	1.0	3.1	0.4	4.5	0.7	4.1
$g_{60}\|t$	8.8	1.2	8.9	1.4	12.9	0.7	14.3	0.7	4.8	2.3	4.4	2.4
$g_{60}\|g_{300}$	1.1	3.1	2.3	2.7	2.2	2.3	1.9	2.5	2.2	3.1	3.9	2.5
$t\|g_{60}$	17.8	0.6	14.1	1.0	12.8	0.7	11.2	1.0	7.0	2.0	11.8	1.5
$t\|t$	33.7	0.0	44.9	0.0	28.8	0.0	33.0	0.0	66.8	0.0	66.0	0.0
$t\|g_{300}$	13.2	0.8	10.3	1.3	10.5	0.9	16.2	0.6	5.2	2.3	6.3	2.1
$g_{300}\|g_{60}$	4.8	1.7	3.2	2.4	4.8	1.6	2.9	2.2	3.4	2.7	0.9	3.9
$g_{300}\|t$	13.8	0.8	11.6	1.2	19.9	0.3	16.5	0.6	8.6	1.8	4.8	2.3
$g_{300}\|g_{300}$	2.8	2.2	2.7	2.5	6.2	1.4	1.1	3.0	1.3	3.5	1.1	3.7

Note: Contributions from the individual enantiomeric pairs are included.

comparison to the *trans–trans* (i.e. $t|t$) conformation (Table 1). The pure *gauche*-containing backbone conformations (i.e. $g_{60}|g_{60}$, $g_{60}|g_{300}$, $g_{300}|g_{60}$ and $g_{300}|g_{300}$) are 1.7–3.1 kcal mol^{-1} less stable than the $t|t$ conformation. O'Reilly and Mosher [9] estimated the relative energies between i-, a- and s-PMMA backbone conformations in 1981 using infrared spectroscopy. This early experimental study provided the following range for the energetic differences between the *trans–trans* and the *gauche*-containing conformations (i.e. $t|t$ vs. $t|g$, $g|t$ and $g|g\}$: 0.680 ± 0.030–0.685 ± 0.075 kcal mol^{-1} for i-PMMA, 1.164 ± 0.080–2.090 ± 0.030 kcal mol^{-1} for s-PMMA and 0.905 ± 0.070–1.430 ± 0.014 kcal mol^{-1} for a-PMMA. Assuming that the high-energy $g|g$ conformation had a negligible contribution to the infrared spectrum, our MD-derived ΔG values are in good agreement with O'Reilly and Mosher's estimates for i- and a-PMMA. However, Tretinnikov and Ohta [26], using more modern infrared spectroscopy techniques over a range of temperatures, estimated that the $t|t$ conformation is more stable than the corresponding $\{g|t + t|g\}$ conformation by 2.51 ± 0.27 and 2.77 ± 0.16 kcal mol^{-1} in i- and s-PMMA. The quantitative disagreement between their i-PMMA results and our MD results could be due to: (a) incomplete conformational sampling during the simulations, (b) experimental error in fitting the energy difference between $t|t$ and $\{g|t + t|g\}$ using integrated absorptivities over a range of temperatures or (c) a combination of (a) and (b). Regardless of the quantitative accuracy, the computed free energy surfaces about ϕ/ψ agree with the experimental trend seen by both research groups, where i-PMMA has a smaller $t|t$ to $\{g|t + t|g\}$ energy difference than a-PMMA.

3.3.3 *Relative importance of individual conformational states*

An often referred to theoretical paper that examines the conformational energetics of the PMMA backbone is by Vacatello and Flory [2]. In that paper, two models are presented (see [2], figure 3IIa and IIb)) that represent i- and s-PMMA, which provide for relative conformational energies. However, a close examination of these two models shows that they are actually the same molecule since they can be interconverted through simple bond rotations, as the molecule lacks an enatiomeric centre. As such, their energetic results are difficult to interpret. What is apparent from their study is that they predict a $t|t$ conformation to be most stable. In the same year, Sundararajan [19] also published theoretical estimates for the backbone energetics. Sundararajan results confirm that the $t|t$ conformation is more stable than its nearest $\{g|t + t|g\}$ conformation, with a computed energetic difference of 0.8 kcal mol^{-1}(i-PMMA) and 0.7 kcal mol^{-1} (s-PMMA). The qualitative observations by both research groups that the $t|t$ conformation is the most stable for both i- and a-PMMA and Sundararajan's quantitative stability for i-PMMA are in agreement with the MD free energy results presented in Table 1. However, we predict a slightly larger energetic difference (1.0 kcal mol^{-1}) between the $t|t$ conformation and its nearest $\{g|t + t|g\}$ conformation (i.e. $t|g_{60}$) for a-PMMA, resulting in the correct relative size ordering of ΔG between $t|t$ and $\{g|t + t|g\}$ for i- and a-PMMA (as discussed in the previous paragraph).

Each of these nine regions is actually composed of two finer elements (Figures 7 and 8). Qualitatively describing the resulting 18 regions requires the inclusion of $+/-$ symbols to the nomenclature presented in Figure 1.[1] Examining the ϕ/ψ population graphs for i- and a-PMMA (Figures 7(b) and 8(b)), it is clear that ϕ/ψ tend to adopt $+/+$ and $-/-$ regions (e.g. $t^+|t^+$ and $t^-|t^-$). This trend was also seen by Sundararajan and Flory [24] and is due to steric hindrance and repulsion that occurs about the $+/-$ and $-/+$ conformations.

Considering these finer regions, i-PMMA populates six conformations non-negligibly (Figure 7(a), (b)), which are in order of most to least populated, $t^+|t^+ > t^+|g^+_{60} > t^-|t^- > g^-_{300}|t^- > t^+|g^+_{300} > g^-_{60}|t^-$.[2] Conversely, a-PMMA populates $t^+|t^+$ and $t^-|t^-$ (Figure 8(a)) to a greater extent, resulting in a comparable loss of the *gauche*-containing conformations (i.e. $g_{60}|t$, $t|g_{60}$, $t|g_{300}$ and $g_{60}|t$). The population distribution and the free energy surfaces shown in Figure 8 represent the sum of all meso (i.e. D–D and L–L) and racemic diads (i.e. D–L and L–D), and also represent the experimentally relevant observable. However, due to our theoretical model, we can gain additional information on how each of these diads contributes to the overall population distribution and free energy surface. Excluding the capping residues, there are a total of 295 ϕ/ψ angle sets that arise from 295 combinations of D and L residues. In the a-PMMA simulation presented here, there are 91 D–D pairs, 71 L–D pairs, 68 D–L pairs and 65 L–L pairs.

Considering only the D–D pairs, the population and free energy surface is very similar to that obtained from the i-PMMA simulation, which contains only the D–D pairs. However, the relative preference ordering is shifted to $g^-_{300}|t^- > t^+|t^+ > t^-|t^- \approx t^+|g^+_{60} > g^-_{60}|t^- > t^+|g^+_{300}$. This may be due to the influence of other diads, where the conformation of L–L, D–L and L–D pairs causes the D–D preference to shift relative to i-PMMA's pure D–D simulation. An alternative possibility is that the simulations have not sampled enough conformational space to obtain statistical convergence in i-PMMA, a-PMMA or in both simulations. The population distribution and free energy surface arising out of the L–L pairs are symmetrically related to those computed by the D–D pairs (Figure 9). However, the population preferences is shifted again to an ordering of $t^-|t^- > t^-|g^-_{300} \approx g^+_{300}|t^+ \approx g^+_{60}|t^+ \approx t^-|t^- > t^-|g^-_{60}$. Such a drastic population shift between symmetrically

related enantiomeric pairs suggests that the simulations have not sufficiently sampled the conformational space. We intend to investigate this further by performing mesoscale coarse-grained simulations, whose entropically enhanced output will be used as the input into additional atomistic simulations.

A very different result is seen for the D–L and L–D pairs, which are also symmetrically related to one another. In both of these cases, there is a very strong preference for a single conformation, which is 65% $t^+|t^+$ for the D–L pairs and 66% $t^-|t^-$ for the L–D pairs (Table 1). As seen in their free energy surfaces, the *gauche*-containing conformations are significantly higher in energy, and collectively contribute 7% (D–L) and 6% (L–D) of the total population. The remaining 26% (D–L) and 27% (L–D) of the population arises from the $\{g|t + t|g\}$ conformations.

From the more detailed enantiomeric pair analysis presented here, it can be concluded that the observed population preference in an experimental a-PMMA melt is a combination of the preference about each of its meso and racemic diads. Experiments [10, 12, 51] and earlier computational [2, 18, 19, 24] studies have observed that a-PMMA and s-PMMA have a strong $t|t$ preference, which must arise from each of the diads. From the current MD study, we can now conclude that the $t|t$ preference in a-PMMA, and most likely in s-PMMA, has a significant contribution from the D–L and L–D racemic diads, and a lesser contribution from the D–D and L–L diads.

4. Conclusion

We have presented in this paper new and reliable atomistic models for MMA and four PMMA residues (i.e. monomer repeating unit) that can be directly used to perform molecular simulations. The PMMA residues themselves can be used to construct isostatic, syndiotactic and atactic PMMA polymers of various lengths. Special attention was given towards deriving the partial atomic charges for MMA and PMMA's residues.

Simulations performed on MMA were used to validate the model and the force field employed in the simulations. The simulations were able to satisfactorily reproduce MMA's experimental density (298 K), enthalpy of vaporisations (280–440 K) and heat capacity (298 K).

The PMMA melt simulations confirmed the previous experimental finding that the backbone exists in a *trans–trans* and *trans–gauche* conformation at temperatures above the glass transition. The population of the *trans–gauche* conformation is expected to increase with increasing temperature due to the statistical weighting factor of four (Equation (4)), which represents the number of accessible *trans–gauche* conformations relative to a *trans–trans* conformation. Both the isotactic and atactic simulations revealed nine general regions occupied in the backbone's ϕ/ψ space, corresponding to combinations of the *trans*, (+)-*gauche* and (−)-*gauche* conformations. Upon closer examination of the simulation results, each of these nine regions is subsequently divided into two finer elements, resulting in 18 total conformational regions, which arise from local steric hindrance and repulsion. Consequently, we have also presented a detailed nomenclature scheme that can be used to fully capture the backbone conformation at atomic resolution.

Through the consideration of these 18 finer regions, we were able to state how much of each region contributed to the overall *trans* and *gauche* conformations adopted by the backbone. Most interestingly, we found that the racemic diads of a-PMMA preferentially formed a *trans–trans* conformation, while the meso diads of i- and a-PMMA preference were distributed over the *trans–trans* and *trans–gauche* conformations. We hope that understanding these conformational subtleties will aid experimentalists in their elucidation of PMMA conformation and behaviour.

Acknowledgements

We would like to thank Axel Arnold for helpful discussions on autocorrelation functions and assistance in generating the population graphs, as well as Astrid Maaß and Florian Müller-Plathe for their insightful discussion on MMA and PMMA.

Notes

1. When a torsion angle populates a value that is less than its ideal *cis*, *gauche*, *anticlinal* or *trans* value (e.g. 55 vs. 60 or 290 vs. 300), it is given a negative sign (e.g. g^-_{60} or g^-_{300}); conversely, when a torsion angle populates a value greater than its ideal angle (e.g. 65 vs. 60 or 310 vs. 300), it is given a positive sign (e.g. g^+_{60} or g^+_{300}).
2. Over 7,000,000 ϕ and ψ angles were recorded for the last 20 ns of each MD simulation involving PMMA, whose values went into computing the population and free energy.

References

[1] J. Brandrup, E.H. Immergut, and E.A. Grulke, *Polymer Handbook*, 4th ed., Vol. 1, Wiley, Hoboken, NJ, 1999.
[2] M. Vacatello and P.J. Flory, *Conformational statistics of poly(methylmethacrylate)*, Macromolecules 19 (1986), pp. 405–415.
[3] D.J. Ward and G.R. Mitchell, *Modeling the structure of a polymer glass poly(methyl methacrylate) through neutron-scattering experiments*, Phys. Scr. T57 (1995), pp. 153–160.
[4] B. Gabrys, J.S. Higgins, and O. Scharpf, *Contamination by coherent scattering of the elastic incoherent structure factor observed in neutron-scattering experiments*, J. Chem. Soc. Faraday Trans. I 82 (1986), pp. 1923–1927.
[5] B. Gabrys, J.S. Higgins, and O. Scharpf, *Short-range order in amorphous poly(methyl methacrylate)*, J. Chem. Soc. Faraday Trans. I 82 (1986), pp. 1929–1934.
[6] R.L. Miller, R.F. Boyer, and J. Heijboer, *X-ray scattering from amorphous acrylate and methacrylate polymers – Evidence of local order*, J. Polym. Sci. B: Polym. Phys. 22 (1984), pp. 2021–2041.

[7] R. Mukhopadhyay, A. Alegria, J. Colmenero, and B. Frick, *Methyl group dynamics in poly(vinylacetate): A neutron scattering study*, Macromolecules 31 (1998), pp. 3985–3993.

[8] K. Schmidt-Rohr, A.S. Kulik, H.W. Beckham, A. Ohlemacher, U. Pawelzik, C. Boeffel, and H.W. Spiess, *Molecular nature of the beta-relaxation in poly(methyl methacrylate) investigated by multidimensional NMR*, Macromolecules 27 (1994), pp. 4733–4745.

[9] J.M. O'Reilly and R.A. Mosher, *Conformational energies of stereoregular poly(methyl methacrylate) by Fourier-transform infrared-spectroscopy*, Macromolecules 14 (1981), pp. 602–608.

[10] R. Lovell and A.H. Windle, *Determination of the local conformation of PMMA from wide-angle X-ray scattering*, Polymer 22 (1981), pp. 175–184.

[11] C.X. Chen, J.K. Maranas, and V. Garcia-Sakai, *Local dynamics of syndiotactic poly(methyl methacrylate) using molecular dynamics simulation*, Macromolecules 39 (2006), pp. 9630–9640.

[12] A.C. Genix, A. Arbe, F. Alvarez, J. Colmenero, W. Schweika, and D. Richter, *Local structure of syndiotactic poly(methyl methacrylate). A combined study by neutron diffraction with polarization analysis and atomistic molecular dynamics simulations*, Macromolecules 39 (2006), pp. 3947–3958.

[13] A.C. Genix, A. Arbe, F. Alvarez, J. Colmenero, B. Farago, A. Wischnewski, and D. Richter, *Self- and collective dynamics of syndiotactic poly(methyl methacrylate). A combined study by quasielastic neutron scattering and atomistic molecular dynamics simulations*, Macromolecules 39 (2006), pp. 6260–6272.

[14] F. Bosscher, G. Tenbrinke, and G. Challa, *Association of stereoregular poly(methyl methacrylates). 6. Double-stranded helical structure of the stereo-complex of isotactic and syndiotactic poly(methyl methacrylate)*, Macromolecules 15 (1982), pp. 1442–1444.

[15] J. Dybal, J. Stokr, and B. Schneider, *Vibrational spectra and structure of stereoregular poly(methyl methacrylate) and of the stereocomplex*, Polymer 24 (1983), pp. 971–980.

[16] O.N. Tretinnikov, *Backbone and ester group conformations of stereoregular poly(methyl methacrylate)s in the stereocomplex*, Macromolecules 36 (2003), pp. 2179–2182.

[17] P. Painter and H. Huang, *Concerning the determination of conformational states in polymers by infrared spectroscopy: A study of poly(methyl methacrylate)*, Macromolecules 41 (2008), pp. 2494–2501.

[18] J. Heijboer, J.M. Baas, B. Vandegraaf, and M.A. Hoefnagel, *A molecular mechanics study on rotational motions of side groups in poly(methyl methacrylate)*, Polymer 28 (1987), pp. 509–513.

[19] P.R. Sundararajan, *Conformational analysis of poly(methyl methacrylate)*, Macromolecules 19 (1986), pp. 415–421.

[20] F.P. Grigor'eva and Yu.Ya. Gotlib, *Internal rotation in the lateral groups and the dielectric polarization of stereoregular polymethyl methacrylate (PMM)*, Poly. Sci. USSR 10 (1968), pp. 396–407.

[21] V. Subramanian, P.S. Asirvatham, R. Balakrishnan, and T. Ramasami, *Molecular mechanics studies on polypropylene and polymethylmethacrylate polymers*, Chem. Phys. Lett. 342 (2001), pp. 603–609.

[22] T.M. Nicholson and G.R. Davies, *Modeling of methyl group rotations in PMMA*, Macromolecules 30 (1997), pp. 5501–5505.

[23] U.M. Apel, R. Hentschke, and J. Helfrich, *Molecular dynamics simulation of syndio- and isotactic poly(methyl methacrylate) in benzene*, Macromolecules 28 (1995), pp. 1778–1785.

[24] P.R. Sundararajan and P.J. Flory, *Configurational characteristics of poly(methyl methacrylate)*, J. Am. Chem. Soc. 96 (1974), pp. 5025–5031.

[25] J.K. Maranas, *The effect of environment on local dynamics of macromolecules*, Curr. Opin. Colloid Interface Sci. 12 (2007), pp. 29–42.

[26] O.N. Tretinnikov and K. Ohta, *Conformation-sensitive infrared bands and conformational characteristics of stereoregular poly(methyl methacrylate)s by variable-temperature FTIR spectroscopy*, Macromolecules 35 (2002), pp. 7343–7353.

[27] H.S. Shin, Y.M. Jung, T.Y. Oh, T.Y. Chang, S.B. Kim, D.H. Lee, and I. Noda, *Glass transition temperature and conformational changes of poly(methyl methacrylate) thin films determined by a two-dimensional map representation of temperature-dependent reflection–absorption FTIR spectra*, Langmuir 18 (2002), pp. 5953–5958.

[28] K.N. Kirschner, A.B. Yongye, S.M. Tschampel, J. Gonzalez-Outeirino, C.R. Daniels, B.L. Foley, and R.J. Woods, *GLYCAM06: A generalizable biomolecular force field. Carbohydrates*, J. Comput. Chem. 29 (2008), pp. 622–655.

[29] I.C. Bayly, P. Cieplak, W. Cornell, and A.P. Kollman, *A well-behaved electrostatic potential based method using charge restraints for deriving atomic charges: The RESP model*, J. Phys. Chem. 97 (1993), pp. 10269–10280.

[30] T. Darden, D. York, and L. Pedersen, *Particle mesh Ewald: An N log(N) method for Ewald sums in large systems*, J. Chem. Phys. 98 (1993), pp. 10089–10092.

[31] U. Essmann, L. Perera, M.L. Berkowitz, T. Darden, H. Lee, and L.G. Pedersen, *A smooth particle mesh Ewald method*, J. Chem. Phys. 103 (1995), pp. 8577–8593.

[32] W.L. Jorgensen, J.D. Madura, and C.J. Swenson, *Optimized intermolecular potential functions for liquid hydrocarbons*, J. Am. Chem. Soc. 106 (1984), pp. 6638–6646.

[33] J. Spevacek and B. Schneider, *NMR-study of structure and dynamics of stereocomplexes of poly(methyl methacrylate) in C_6D_6 and CD_3CN*, Colloid Polym. Sci. 258 (1980), pp. 621–625.

[34] D.A. Case, T.A. Darden, T.E. Cheatham, III, C.L. Simmerling, J. Wang, R.E. Duke, R. Luo, K.M. Merz, D.A. Pearlman, M. Crowley, R.C. Walker, W. Zhang, B. Wang, S. Hayik, A. Roitberg, G. Seabra, K.F. Wong, F. Paesani, X. Wu, S. Brozell, V. Tsui, H. Gohlke, L. Yang, C. Tan, J. Mongan, V. Hornak, G. Cui, P. Beroza, D.H. Mathews, C. Schafmeister, W.S. Ross, and P.A. Kollman, *AMBER 9*, University of California, San Francisco.

[35] M.S. Gordon and M.W. Schmidt, *Advances in electronic structure theory: GAMESS a decade later*, in *Theory and Applications of Computational Chemistry: The First Forty Years*, C.E. Dykstra, G. Frenking, K.S. Kim, and G.E. Scuseria, eds., Elsevier, Amsterdam, 2005, pp. 1167–1189.

[36] D.L. Beveridge and F.M. DiCapua, *Free energy via molecular simulation: Applications to chemical and biomolecular systems*, Annu. Rev. Biophys. Biophys. Chem. 18 (1989), pp. 431–492.

[37] B.L. Baker, M. Orgill, N.L. Owen, E.H. Stephenson, G.A. Williams, J.N. Macdonald, and J.E. Boggs, *The molecular conformation of methyl methacrylate – An infrared and* ab initio *study*, J. Mol. Struct. 356 (1995), pp. 95–104.

[38] V. Santhanam, S. Singh, and J. Sobhanadri, *Conformational analysis of some acrylates using dipole moment calculations by CNDO/force method*, Tetrahedron 29 (1983), pp. 4183–4187.

[39] T. Tsuji, H. Ito, H. Takeuchi, and S. Konaka, *Molecular structure and conformation of methyl methacrylate determined by gas electron diffraction*, J. Mol. Struct. 475 (1999), pp. 55–63.

[40] A. Virdi, V.P. Gupta, and A. Sharma, Ab initio *studies on conformation, vibrational and electronic spectra of methyl methacrylate*, J. Mol. Struct.: Theochem 634 (2003), pp. 53–65.

[41] E. Hollauer, M.L. Rocco, M.C. Lopes, and G.G. de Souza, *An* ab initio *study of the valence excitation of methyl methacrylate as observed by EELS*, J. Electron Spectrosc. Relat. Phenom. 104 (1999), pp. 31–39.

[42] Private Communication: Evonik Roehm GmbH, Methylmethacrylate MMA: Datenblatt AM 001, July 1997, Kirschenallee, Darmstadt.

[43] W.V. Steele, R.D. Chirico, A.B. Cowell, S.E. Knipmeyer, and A. Nguyen, *Thermodynamic properties and ideal-gas enthalpies of formation for trans-methyl cinnamate, α-methyl cinnamaldehyde, methyl methacrylate, 1-nonyne, trimethylacetic acid, trimethylacetic anhydride, and ethyl trimethyl acetate*, J. Chem. Eng. Data 47 (2002), pp. 700–714.

[44] A.M. Alb, P. Enohnyaket, M.F. Drenski, A. Head, A.W. Reed, and W.F. Reed, *Online monitoring of copolymerization involving comonomers of similar spectral characteristics*, Macromolecules 39 (2006), pp. 5705–5713.

[45] A.M. Alb, P. Enohnyaket, M.F. Drenski, R. Shunmugam, G.N. Tew, and W.F. Reed, *Quantitative contrasts in the copolymerization of acrylate- and methacrylate-based comonomers*, Macromolecules 39 (2006), pp. 8283–8292.

[46] E. Erdös, L. Jäger, and J. Pouchy, *Specificka tepla methylesteru a butylesteru kyseliny methakrylove*, Chem. Listy 46 (1952), p. 770.
[47] M. Karabaev, T.P. Abduzhaminov, A.A. Saidov, and Kh.T. Igamberdyev, *Thermophysical properties of liquid methacrylic acid and its simple esters*, Izv. Akad. Nauk Uzb. SSR Ser. Fiz.-Mat. Nauk 4 (1985), pp. 71–74.
[48] T.P. Melia, *Part VIII-Methylmethacrylate and polymethylmethacrylate*, Polymer 3 (1962), pp. 317–319.
[49] D. Zhang, G.C. Benson, M.K. Kumaran, and B.C.-Y. Lu, *Excess thermodynamic properties for methyl methacrylate + methanol and +ethanol*, J. Chem. Thermo. 18 (1986), pp. 149–158.
[50] H. Kusanagi, H. Tadokoro, and Y. Chatani, *Double strand helix of isotactic poly(methyl methacrylate)*, Macromolecules 9 (1976), pp. 531–532.
[51] O.N. Tretinnikov, *Conformational characteristics of stereoregular PMMA and of the stereocomplex: New insights from FTIR measurements*, Macromol. Symp. 203 (2003), pp. 57–69.